Determination of the layer structure of embedded strained InGaAs multiple quantum wells by high resolution x-ray diffraction

Woo-Young Choi and Clifton G. Fonstad
Department of Electrical Engineering and Computer Science, Massachusetts Institute of Technology, Cambridge, Massachusetts 02139

(Received 4 January 1993; accepted for publication 9 March 1993)

High resolution x-ray diffraction (HRXRD) has been used to determine the layer compositions and thicknesses of compressively strained InGaAs multiple-quantum-well (MQW) structures embedded in thick cladding layers that are nominally lattice matched to InP. The entire layer structure was accurately determined from the results of HRXRD measurements for a simple strained MQW structure in which barriers and claddings are of the same composition. The estimated margins of error are less than 1% for the quantum-well indium composition and ±2.5 Å for well and barrier thicknesses. The layer structure of the active region in a complete InGaAlAs graded-index separate confinement strained MQW laser diode has also been determined by HRXRD.

The utility of high resolution x-ray diffraction (HRXRD) for the structural assessment of epitaxially grown semiconductor layers is now well established. Among layer structures characterized by HRXRD, those with multiple quantum wells (MQWs) or superlattices have received much attention since quantum confinement effects in such structures are the basis of many advanced heterostructure devices. In x-ray investigation of these structures, the compositions and thicknesses of wells and barriers can be accurately determined from the analysis of satellite peaks caused by the artificially added periodicity.[1] In this letter, we report the results of a HRXRD investigation of compressively strained InGaAs MQWs embedded in thick nominally lattice-matched top and bottom cladding layers. The interest for investigating such structures by HRXRD stems from their utility for such device applications as strained MQW laser diodes and modulators.

Figure 1 shows two layer structures used for the present HRXRD study with their target composition and thickness values. Sample A is a *p-i-n* structure with four compressively strained quantum wells and quaternary InGaAlAs barriers and claddings of the same composition. Sample B is an actual device structure for graded-index separate confinement (GRINSCH) strained MQW laser diodes. The goal of the investigation was to determine the compositions and thicknesses of wells and barriers in these structures from the results of HRXRD measurements. The samples are two of many samples with different strained MQW structures grown in order to optimize the strained MQW structure for 1.5 μm laser diodes. The growth was done on (001) InP wafers by molecular beam epitaxy (MBE); the details of MBE growth for strained MQW structures can be found elsewhere.[2]

The HRXRD measurements were done on a commercially available Bede model 300 two-crystal system from Bede Scientific Instruments Limited. The Cu-$K\alpha$ radiation was generated by a Rigaku RU200 generator with the bias voltage and the beam current set at 60 kV and 200 mA, respectively. An InP substrate oriented for the (004) reflection was used for the first crystal. Rocking curves were measured for symmetric (004) reflection with the goniometer increment of 2 arcsec and the count time of 2 s.

Figure 2 shows measured and simulated HRXRD spectra of sample A (the details of the simulation are discussed later). The satellite peaks in the data show the $[\sin(4x)/\sin(x)]^2$ dependence predicted by the theory.[3,4] In order to analyze these data, it is first necessary to understand how x-ray diffraction from embedded strained MQWs is affected by the surrounding claddings. This is done by separating the total diffracted x-ray field into three different parts as

$$E_{\text{total}}(\Theta)=E_b(\Theta)+E_{\text{MQW}}(\Theta)\exp(iT_b)+E_t(\Theta)\exp[i(T_b+T_{\text{MQW}})],$$

where E_b and E_t correspond to the diffracted x-ray fields due to the bottom and top cladding layers, respectively, and E_{MQW} to that of the MQW region. E_b, E_t, and E_{MQW} are in general complex quantities and depend on the incident x-ray angle, Θ. For our analysis, only one polarization is considered and the dynamic effects are not considered. T_b and T_{MQW} are the layer thickness of the bottom cladding and the MQW region, respectively. Phase factors are introduced to account for the spacial shifts of the MQW region and the top cladding layer. This separation is shown schematically in Fig. 3. The measured x-ray intensity is then

$$\begin{aligned}|E_{\text{total}}|^2=&|E_b|^2+|E_{\text{MQW}}|^2+|E_t|^2+2|E_{\text{MQW}}|\\&\times\cos(T_b+\theta_{b,\text{MQW}})\\&+2|E_bE_t|\cos(T_b+T_{\text{MQW}}+\theta_{b,t})\\&+2|E_{\text{MQW}}E_t|\cos(T_{\text{MQW}}+\theta_{\text{MQW},t}),\end{aligned}$$

where $\theta_{b,\text{MQW}}$, $\theta_{b,t}$, and $\theta_{\text{MQW},t}$ represent the phase differences between corresponding x-ray fields. From the above expression, it can be easily observed that the product terms representing coupling between x-ray fields from different layers have significant contributions only in the range of Θ where $|E_b|$ or $|E_t|$ is significant. In typical HRXRD scans of embedded strained MQW structures, most dominant

 0003-6951/93/222815-03$06.00

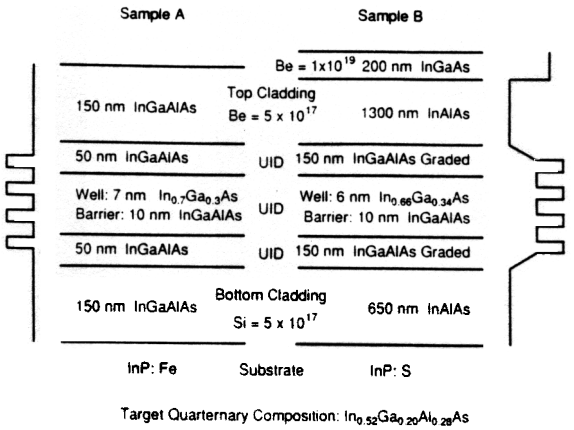

FIG. 1. Layer structures for samples A and B with target compositions and thicknesses. All the InGaAlAs quaternary layers have the same target compositions as shown in the figure. The GRINSCH layers in sample B are linearly graded from $In_{0.52}Al_{0.48}As$ to $In_{0.52}Ga_{0.20}Al_{0.28}As$. InGaAs and InAlAs layers have the lattice matching target compositions, $In_{0.53}Ga_{0.47}As$ and $In_{0.52}Al_{0.48}As$, respectively.

satellite peaks are located away from the cladding peak and, consequently, they are easily resolvable and can be described by the analytical expression derived from MQWs without cladding layers.[3,4] This is different from the case of lattice-matched MQWs embedded in thick cladding layers in which the satellite peaks are not as easily resolvable and suffer more severe interference from the cladding layers. Although the effect of the substrate is neglected in the above analysis, it can be treated just like another cladding layer and the same results can be obtained.

For the complete determination of the strained MQW structure in sample A, it is necessary to determine four independent parameters: well composition, or the vertical lattice spacing inside the wells ($a_{\perp,w}$); well thickness, or the number of monolayers inside the wells (N_w); barrier composition, or the vertical lattice spacing inside the barriers ($a_{\perp,b}$); and barrier thickness, or the number of monolayers inside the barriers (N_b). It is assumed that wells and

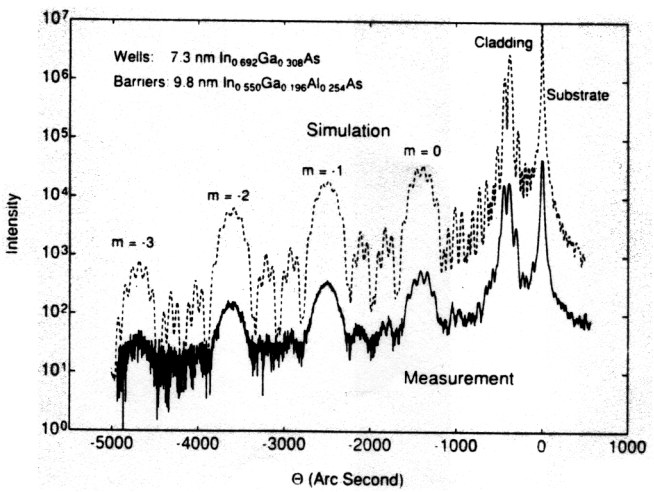

FIG. 2. Measured and simulated HRXRD scans of sample A. The input parameters for simulation that are determined from the analysis are shown in the figure.

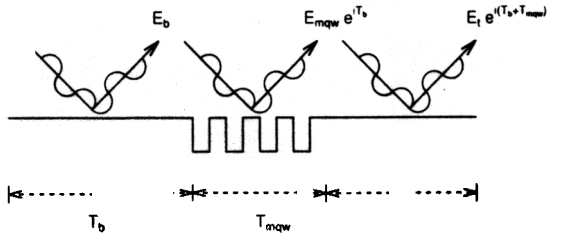

FIG. 3. Schematic diagram for separating an embedded strained MQW structure into three different regions: bottom cladding, wells and barriers, and top cladding. Notice that T_{MQW} is defined as the thickness of four wells and four barriers.

barriers are of identical composition and thickness, respectively, a situation which can be easily achieved with MBE. Further, it is assumed that there is no strain relaxation inside the wells and all the strains are coherently incorporated by tetragonal distortion. This is evidenced by the sharp satellite peaks in the HRXRD scan and a narrow and a strong excitonic photoluminescence peak with full width at half-maximum of 6.5 meV at 10 K from sample A. The task is then reduced to obtaining four independent equations involving the above four parameters. This can be done in the following manner.

(1) Since the barriers and claddings are of the same composition, $a_{\perp,b}$ can be determined from the separation between cladding and substrate peaks in the HRXRD scan.

(2) The position of the zeroth-order satellite peak should correspond to the average vertical lattice spacing in the strained MQW region, $a_{\perp,0}$, or

$$a_{\perp,0}=\frac{N_w\times a_{\perp,w}+N_b\times a_{\perp,b}}{N_w+N_b}$$

where $a_{\perp,0}$ can be easily determined from the position of the zeroth-order satellite peak. If the zeroth-order peak is located close to the cladding peak, then the positions of higher order peaks can be used to determine the correct zeroth-order peak position without the interference of the cladding layers.

(3) From the known expression for the satellite peak periodicity,[4] we obtain

$$\Lambda=\frac{\lambda}{2\cos(\theta)\Delta\theta},$$

where Λ is the spacial periodicity in MQWs ($=N_w d_w+N_b d_b$), λ x-ray wavelength, $\Delta\theta$ the separation between two adjacent satellite peaks, and θ is the angle around which the satellite peak separation is determined.

(4) Finally, the total epilayer thickness t can be expressed as

$$t=\gamma N_b a_{\perp,b}+n\Lambda,$$

where n is the number of quantum wells and γ corresponds to the ratio of the total cladding thickness to the barrier which can be easily determined from the target growth durations for claddings and barriers. The total epilayer

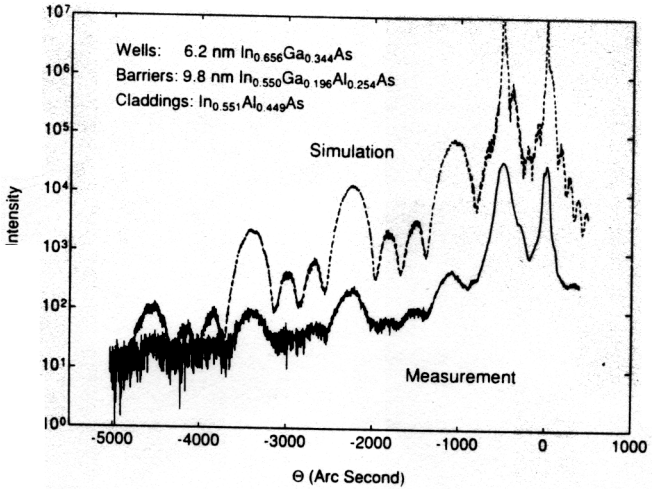

FIG. 4. Measured and simulated HRXRD scans of sample B. The input parameters for simulation that are determined from the analysis are shown in the figure.

thickness can be measured by a profilometer measurement on a step created by selectively etching the epilayer.

By simultaneously solving the above four equations, it is possible to uniquely determine all four parameters, $a_{\perp,w}$, N_w, $a_{\perp,b}$, and N_b. To determine the quaternary composition for barriers and claddings from $a_{\perp,b}$ the band gap of the quaternary was measured from low temperature photoluminescence (1.10 eV at 10 K) and the corresponding composition was calculated. The resulting layer structure is 73 Å $In_{0.692}Ga_{0.308}As$ for the wells and 98 Å $In_{0.550}Ga_{0.196}Al_{0.254}As$ for the barriers. Using these values, a simulation was done with a commercially available software package called RADS (Rocking Curve Analysis by Dynamic Simulation) supplied by Bede Scientific Instruments Limited, and the result is shown in Fig. 2. No iterative changes in input parameters were performed to obtain better matching between measurement and simulation. The matching as shown is excellent, indicating the accuracy of the analysis. It should be noted that the determined values are the average values over the sample area probed by the x-ray beam, which is about 1 mm by 1 mm.

To estimate the margin of error involved in the analysis, an error analysis was performed. The major sources of uncertainties were considered to be in determining the exact peak positions from the x-ray data (± 10 arcsec in an enlarged figure) and the epilayer thickness from a profilometer measurement (± 100 Å or about $\pm 2\%$). By calculating compositions and thickness from the input parameters that span the entire uncertainty range, histograms of possible compositions and thicknesses were obtained. From these, it can be said that the well indium compositions is in the range of 0.692 ± 0.005 (or $\pm 0.7\%$) with 79% confidence, and the well barrier thicknesses are 73 ± 2.5 Å (or $\pm 3.4\%$) and 98 ± 2.5 Å (or $\pm 2.6\%$), respectively, both with 73% confidence. The larger margin of error in thickness than composition is due to the large uncertainty in thickness measurement by the profilometer, which is the accuracy limiting factor.

Figure 4 shows the results of HRXRD measurement and simulation for a complete laser diode structure of sample B. Broad area laser devices made out of this sample lase with threshold current density of about 900 A/cm^2 for 1-mm-long uncoated cavities under pulsed current excitation at room temperature. Due to the complex layer structure, the entire layer structure cannot be determined by HRXRD results alone. However, the same values for barrier composition and thickness as in sample A can be used for sample B, since both samples were grown on the same day with the same target values for barrier composition and thickness. Also, it can be assumed without too much difficulty that the initial 98 Å of the top GRINSCH region has the same composition as the barrier, providing four complete quantum wells and barriers as required. Two remaining conditions are obtained from the satellite peak periodicity and the zeroth-order satellite peak position. Then, the laser diode active region structure can be completely determined, as shown in Fig. 4. For the simulation, the top contact layer was assumed to be lattice matched ($In_{0.53}Ga_{0.47}As$) and the top and bottom GRINSCH regions were each modeled by five layers of constant compositions linearly varying from the barrier quaternary to InAlAs cladding. With the exceptions of the broader cladding layer peak and larger background noise, the agreement between measurement and simulation is excellent, indicating the accuracy of the analysis for a complete laser diode structure. The broad InAlAs peak is probably due to not optimal structural quality of thick InAlAs layers.[5]

By comparing the target layer structure with that determined by HRXRD, we can verify that the effusion cell temperatures were set correctly for desired material compositions with the exception of the aluminum cell, whose temperature should have been higher by about 6 °C. This information can be used for the subsequent MBE growths for a better control of cell temperatures. In addition, the accurate device structure determination by HRXRD as was done for sample B is essential for the correct analysis of device characteristics. In these regards, HRXRD characterization is essential for successful growth of InGaAlAs materials on InP and, in particular, for strained MQWs for device applications.

The authors would like to thank Dr. Brian Bennett at Naval Research Laboratory for helpful discussions on x-ray analysis and Joe Adario at MIT Center for Material Science and Engineering for kindly providing the computing facilities for the x-ray simulations done for this work. This work was funded by JSEP through the MIT Research Laboratory of Electronics, Contract No. DAAL03-92-0001, and by DARPA through the National Center for Integrated Photonics Technology, Subcontract No. 542383.

[1] J. M. Vandenberg, R. A. Hamm, M. B. Panish, and H. Temkin, J. Appl. Phys. **62**, 1278 (1987).
[2] W.-Y. Choi and C. G. Fonstad, J. Cryst. Growth **127**, 555 (1993).
[3] A. Segmüller and A. E. Blakeslee, J. Appl. Cryst. **6**, 19 (1973).
[4] V. Swaminathan and A. T. Macrander, *Material Aspects of GaAs and InP-Based Structures* (Prentice-Hall, Englewood Cliffs, NJ, 1991), Chap. 3.
[5] E. Tournié, Y.-H. Zhang, N. J. Pulsford, and K. Ploog, J. Appl. Phys. **70**, 7362 (1991).